

Quenched binary Bose-Einstein condensates: spin domain formation and coarsening

S. De, D. L. Campbell, R. M. Price, A. Putra, B. M. Anderson, and I. B. Spielman
*Joint Quantum Institute, University of Maryland and National Institute
of Standards and Technology, College Park, Maryland, 20742, USA*
(Dated: December 3, 2024)

We explore the time evolution of quasi-1D two component Bose-Einstein condensates (BEC's) following a quench from one component BEC's with a $U(1)$ order parameter into two component condensates with a $U(1) \times Z_2$ order parameter. In our case, these two spin components have a propensity to phase separate, *i.e.*, they are immiscible. Remarkably, these spin degrees of freedom can equivalently be described as a single component attractive BEC. A spatially uniform mixture of these spins is dynamically unstable, rapidly amplifying any quantum or pre-existing classical spin fluctuations. This coherent growth process drives the formation of numerous spin polarized domains, which are far from the system's ground state. At much longer times these domains grow in size, coarsening, as the system approaches equilibrium. The experimentally observed time evolution is fully consistent with our stochastic-projected Gross-Pitaevskii calculation.

PACS numbers: 75.75.+a, 75.40.Gb

Ultracold atomic gases are unique systems for studying phase transitions where the full range from adiabatic to diabatic can be easily accessed in the laboratory. A prime example of this is the transition from superfluid (SF) to Mott-insulator (MI) in an optical lattice: when the transition is crossed slowly, a nearly $T = 0$ SF transforms into a nearly $T = 0$ MI [1]; however, when the system is quenched by rapidly entering the MI regime, it exhibits rapid dynamics before dephasing into a highly excited, high temperature final state [2–4]. Here we study a similar quantum quench in a two component spinor BEC, where the spin degree of freedom is initialized in a highly excited state. We follow the resulting rapid dynamics during which spin domains first form, and subsequently slowly relax towards equilibrium as the domain size increases and the domain number decreases (see Fig 1). To our knowledge, this is the first observation of domain coarsening [5] in a spinor BEC.

The establishment of out of equilibrium domains formed by quenching through a phase transition is ubiquitous in physical systems ranging from grain formation in minerals [6], structure growth in the early universe [7], to domain formation in magnetic systems. For an initially zero-temperature system, a quench can result from rapidly traversing a second order quantum phase transition that is associated with a change in the system's symmetry. In the case of a quench from SF to MI, the SF's $U(1)$ order parameter is absent in the MI phase (with its trivial Z_1 order parameter). In contrast, the order parameter transforms from Z_1 to Z_2 for a quenched transverse-field Ising ferromagnet [8]. In our experiment, we prepare a transversely magnetized two component spinor BEC described by a $U(1)$ order parameter, and observe the formation and spatial expansion (coarsening) of domains following a quench into a phase with a $U(1) \times Z_2$ order parameter [9, 10], unexplored by previous studies with binary condensates (miscible [11, 12] or immiscible [13, 14]) with their asymmetric Hamiltonians.

As compared with three component systems [15–19], the relative simplicity present here allows us to identify an intriguing analogy between our spin system and a single-component *attractive* BEC as it collapses [20–22].

Here, we explore the time-evolving magnetization of two-component ^{87}Rb Bose-Einstein condensates (BEC's) in the $5S_{1/2}$ electronic ground state. Our BEC's are well described in terms of a spinor wave-function $\Psi(\mathbf{r}) = \{\psi_{\uparrow}(\mathbf{r}), \psi_{\downarrow}(\mathbf{r})\}$, where the $|\uparrow, \downarrow\rangle$ pseudo-spins label $|f=1, m_F = \pm 1\rangle$ atomic spin states. The dynamics of this wave function are given by the spinor Gross-Pitaevskii equation (sGPE)

$$i\hbar\partial_t\psi_{\uparrow,\downarrow}(\mathbf{r}) = \left[-\frac{\hbar^2\nabla^2}{2m} + V(\mathbf{r}) + (c_0 - c_2)n(\mathbf{r}) \right. \quad (1) \\ \left. + 2c_2N|\psi_{\uparrow,\downarrow}(\mathbf{r})|^2 \right] \psi_{\uparrow,\downarrow}(\mathbf{r}) + \frac{\Omega_{\perp}}{2}\psi_{\downarrow,\uparrow}(\mathbf{r}),$$

a continuum analog to the transverse field Ising model. In this expression, $n(\mathbf{r}) = N[|\psi_{\uparrow}(\mathbf{r})|^2 + |\psi_{\downarrow}(\mathbf{r})|^2]$ is the total density; m is the atomic mass; $V(\mathbf{r})$ is a spin-independent external potential; Ω_{\perp} describes the Zeeman shift of a “transverse” magnetic field; and $c_{0,2}$ are the spin-independent and spin-dependent interaction coefficients [23, 24]. In ^{87}Rb 's $f = 1$ manifold, $c_0 = (100.86) \times 4\pi\hbar^2 a_B / m$ vastly exceeds $c_2 \approx -4.7 \times 10^{-3} c_0$, where a_B is the Bohr radius. For a static density profile and when $\Omega_{\perp} = 0$, each spin component in Eq. (1) is separately described by an attractive single-component GPE.

We produce nearly pure $N = 7.0(5) \times 10^5$ atom ^{87}Rb BEC's [28] in the $|f=1, m_F=0\rangle$ hyperfine state, originating from cold $|f=1, m_F=-1\rangle$ thermal clouds formed in a hybrid magnetic/optical trap [25]. These BEC's are subject to a uniform magnetic field with magnitude $B_0 = 107.0(2) \mu\text{T}$ and are confined in the extremely anisotropic crossed optical dipole trap [29] depicted in Fig. 1a. The radial (\mathbf{e}_r , *i.e.*, in the $\mathbf{e}_x - \mathbf{e}_y$ plane) and

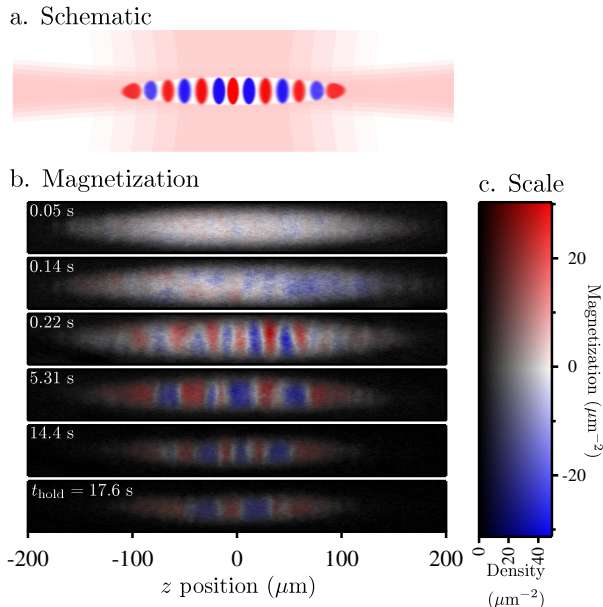


FIG. 1: Magnetization $M_z(\mathbf{r})$. (a) Schematic representation of our experiment, illustrating a spinor BEC with domains in an anisotropic crossed-dipole trap. (b) Images showing the progression from an initially uniformly magnetized condensate (short times) in which domains appear (intermediate times), and then grow spatially (long times); during this whole process the condensate slowly decays away. (c) The color scale indicates both the degree of magnetization (colors from blue to red), and the number density (intensity from black to colored).

axial (\mathbf{e}_z) trap frequencies are $\omega_r/2\pi = 135(3)$ Hz and $\omega_z/2\pi = 3.1(2)$ Hz respectively. Our $T = 90(8)$ nK condensates have radial and axial Thomas-Fermi radii [30] of $R_r = 3.9(1)$ μm and $R_z = 170(7)$ μm .

Because the typical $c_0 n(\mathbf{r})$ spin-independent energy vastly exceeds the $c_2 n(\mathbf{r})$ spin-dependent energy scale, we make the conventional Thomas-Fermi approximation for the overall density distribution $n(\mathbf{r})$ characterized by a chemical potential μ , and a minimum healing length $\xi = \hbar/\sqrt{2m\mu}$. This gives $n(\mathbf{r}) = [\mu - V(\mathbf{r})] / [c_0 + c_2 M_z^2(\mathbf{r})]$, which depends very weakly on the z component of local magnetization vector, $\mathbf{M}(\mathbf{r}) = \{M_x(\mathbf{r}), M_y(\mathbf{r}), M_z(\mathbf{r})\} = \left\{ 2\text{Re}[\psi_\uparrow^*(\mathbf{r})\psi_\downarrow(\mathbf{r})], 2\text{Im}[\psi_\uparrow^*(\mathbf{r})\psi_\downarrow(\mathbf{r})], |\psi_\uparrow(\mathbf{r})|^2 - |\psi_\downarrow(\mathbf{r})|^2 \right\}$.

The spin degrees of freedom vary almost exclusively with axial position [19] because our extremely anisotropic condensate's ≈ 3.9 μm radial extent is comparable to the minimum spin healing length $\xi_s = \xi|c_0/c_2|^{1/2} = 3.20(4)$ μm . Theoretically, we may describe the spin degree of freedom as 1D spinor with components $\chi_{\uparrow,\downarrow}(z) = |\chi_{\uparrow,\downarrow}(z)| e^{i\phi_{\uparrow,\downarrow}(z)}$; retaining terms through first order in c_2/c_0 , we obtain an effective 1D sGPE

$$i\hbar\partial_t\chi_{\uparrow,\downarrow} = \left[-\frac{\hbar^2\partial_z^2}{2m} - g_{1D}(z) + 2g_{1D}(z)|\chi_{\uparrow,\downarrow}|^2 \right] \chi_{\uparrow,\downarrow}. \quad (2)$$

The 1D interaction strength $g_{1D}(z) \propto c_2$ is related to a 1D healing length $\xi_{1D} \approx \sqrt{3/2}\xi_s$. These two 1D sGPE's

are coupled by the local constraints $|\chi_\uparrow(z)|^2 + |\chi_\downarrow(z)|^2 = 1$ and $\phi_\uparrow(z) + \phi_\downarrow(z) = 0$ (i.e., no mass currents). To make the analogy explicit, we have dropped terms quadratic in $|\chi_{\uparrow,\downarrow}|^2$ that result from integrating out the transverse dimensions. These repulsive terms do not affect the spectrum at short times after the quench, but must be included at long times.

Our spinor experiment is initiated by a 34 μs rf-pulse that puts each atom into an equal-amplitude coherent superposition of the $|\uparrow, \downarrow\rangle = |m_F = \pm 1\rangle$ spin states, the ground state when the transverse field Ω_\perp is large; the system then evolves according to Eq. (1) with $\Omega_\perp = 0$. This procedure is therefore equivalent to rapidly quenching Ω_\perp to zero: the ground state goes from breaking a U(1) symmetry to breaking a *different* U(1) along with a Z_2 symmetry (leaving behind a “sneaky” U(1) symmetry). The quenched binary mixture is held for a variable duration t_{hold} , up to 20 s, while spin structure forms and evolves. Spin mixing collisions are suppressed because the relatively large 82 Hz quadratic Zeeman shift greatly exceeds the $c_2 n(\mathbf{r}) \approx 6$ Hz spin dependent energy [15]. As a result, we observe no population in $m_F = 0$ for the entire duration of our experiment. After t_{hold} , we remove the confining potential and allow the atomic ensemble to expand (largely transversely) for 19.3 ms, during which time we Stern-Gerlach [26] separate the spin components. We detect the resulting density distribution by absorption imaging, and reconstruct both $M_x(x, z)$ and $M_z(x, z)$, projected onto the $\mathbf{e}_z - \mathbf{e}_x$ imaging plane [31]. Representative reconstructions of $M_z(x, y)$ at six hold times are depicted in Fig. 1b.

The initially ($t_{\text{hold}} = 0$) uniform $\chi(z) = (|\uparrow\rangle + |\downarrow\rangle)/\sqrt{2}$ spin superposition is dynamically unstable (as indicated in Fig. 1b's snapshots). At this unstable point, small spin-wave excitations have an $(\hbar\omega/\mu_{1D})^2 = (k\xi_{1D})^2 [(k\xi_{1D})^2 - 2]$ energy spectrum [5], where $\mu_{1D} = \hbar^2/2m\xi_{1D}^2$ is a typical 1D spin interaction energy. When $\hbar\omega$ is imaginary – for $k\xi_{1D} \in (0, \sqrt{2})$ – the associated modes grow exponentially with peak gain at $k = 1/\xi_{1D}$, amplifying any existing spin fluctuations, classical or quantum. Figure 2 depicts the magnetization $M_z(z)$, showing the initially unmagnetized condensate develop visible structure after about 200 ms. The experimental data plotted in Fig. 2a is in near perfect agreement with a stochastic-projective GPE (SP-GPE) simulation [27], with parameters nearly matched to our experiment, Fig. 2b.

While the amplitude of these spin waves (grow with an exponential time constant $\tau(k) = 1/\text{Im}(\omega(k, z))$ [minimum at $\tau(z) = 2m\xi_{1D}^2(z)/\hbar \approx 42$ ms], Fig. 2 shows that no structure is visible until $t_{\text{hold}} \approx 200$ ms. Our simulations confirm that structure begins to grow immediately, and only technical noise prevents us from detecting the growing spin modulation at shorter times. Figure 2 also shows that spin structure forms more slowly in the lower

density periphery of the system where ξ_{1D} and therefore τ are larger. To quantify this effect, Fig. 3 depicts the number of spin-regions visible above the noise. This number, increasing for short times, is plotted along with the results of our SP-GPE simulations, and a local density approximation (LDA, accounting for our systems inhomogeneous density profile) prediction for the expected pattern of domain growth.

The spin modulations continue to grow in amplitude until, at $t_{\text{hold}} \approx 300$ ms, they form fully spin polarized domains of $|\uparrow\rangle$, and $|\downarrow\rangle$, with a spacing set by the dynamic growth process, not by the system's equilibrium thermodynamics. After this period of rapid growth, the polarized spin domains evolve slowly, equilibrating, for the remaining 20 s duration of our experiment [32].

Our BEC has a $\tau = 10(1)$ s lifetime, implying that the domain pattern *must* evolve in time as the BEC slowly contracts. The simplest model – in which the domain pattern contracts in lock-step with the dwindling BEC – is obviated by Fig. 3, that shows the number of domains decreasing after $t_{\text{hold}} \approx 1$ s. Indeed, once a domain becomes smaller than $\approx 2\xi_{1D}(z)$, it can no longer reach full spin-polarization in its center, and it therefore ceases to be a barrier for the hydrodynamic flow of the other spin state. As a result, small domains de-pin and can move freely until they coalesce with another domain of the same spin.

While Figs. 2 and 3 qualitatively suggest that the domains gradually expand as t_{hold} increases from 300 ms to 20 s, it is difficult to obtain a quantitative mea-

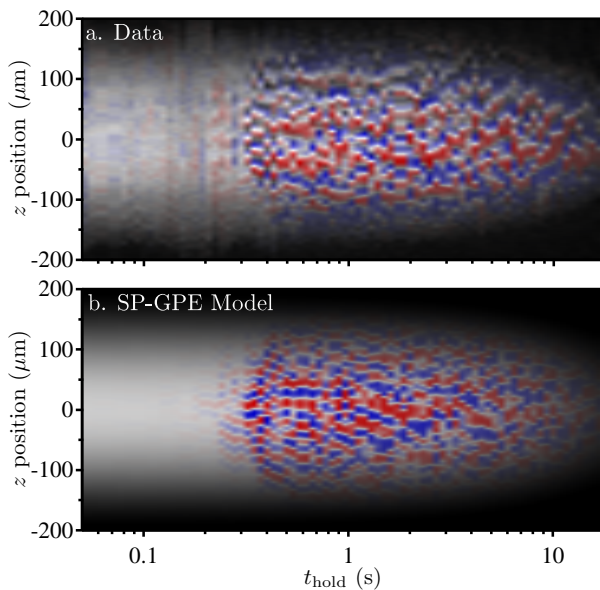


FIG. 2: Time evolution of magnetization $M_z(z)$. (a) Experimental data and (b) finite temperature simulation using the SP-GPE method. In both simulation and experiment, the spatial structure of $M_z(z)$ coarsens after an initial growth period as domains coalesce.

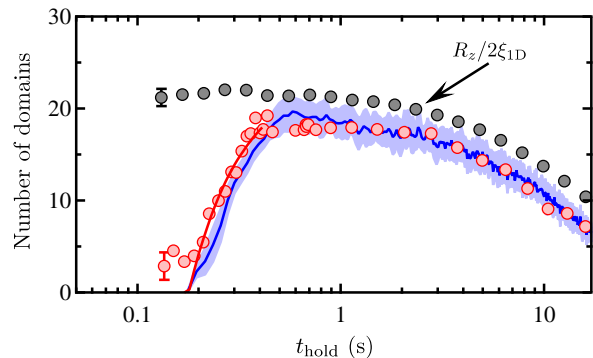


FIG. 3: Number of domains as a function of t_{hold} . The red symbols depict the experimentally observed number of domains (typical uncertainty plotted on the leftmost point) and the blue curve plots the results of our SP-GPE simulation (uncertainties denoted by the blue band). In both cases, the uncertainties reflect the standard deviation over many realizations. In addition, the red curve fits the data to a model assuming exponential growth along with a non-zero observation threshold, in the LDA. The grey symbols correspond to the ratio $R_z/2\xi_{1D}$: an estimate of domain number, assuming the system with length $2R_z$ is partitioned into domains of size $4\xi_{1D}$.

sure of domain size from data in this form. Indeed, the data show that while measurements at neighboring times have similar domain sizes, the exact domain pattern has a significant element of randomness – primarily in the form of phase shifts – likely resulting from subtle differences in the initial conditions, as amplified by the subsequent exponential gain process. To mitigate these effects, we turn to the power spectral density $\text{PSD}_{x,z}(k) = \left| \int M_{x,z}(z) \exp(ikz) dz \right|^2$ obtained from these data. With the PSD, we can compare different realizations even in the presence of spatial phase shifts of the domain structure.

Figure 4a shows $\text{PSD}_z(k)$ derived from $M_z(z)$ shown in Fig. 2. For short times ($t_{\text{hold}} \lesssim 300$ ms), a narrow peak associated with the growing spin modulations develops. Once the spin domains reach unity polarization, the magnetization's magnitude saturates and the boundaries between domains – domain walls – sharpen, broadening $\text{PSD}_z(k)$ starting at $t_{\text{hold}} \approx 300$ ms. At longer times, the broad peak drifts to smaller wave-vector, indicating an increasing typical domain size. Figure 4b compares this peak location for both experiment and theory (red and blue symbols respectively, showing nearly identical behavior) against $1/\xi_{1D}$. Our simple model predicts maximum gain at this wave-vector, however, the peak in $\text{PSD}_z(k)$ for both the experiment and the SP-GPE is at slightly smaller k . This results from the inhomogeneous density profile of the spinor BEC: simulations of uniform systems do show peak gain at $1/\xi_{1D}$.

Unlike $\text{PSD}_z(k)$, $\text{PSD}_x(k)$ is peaked about zero; this is because $M_x(z)$ is only appreciable in the domain walls where the gas is not fully polarized: it is a series of nar-

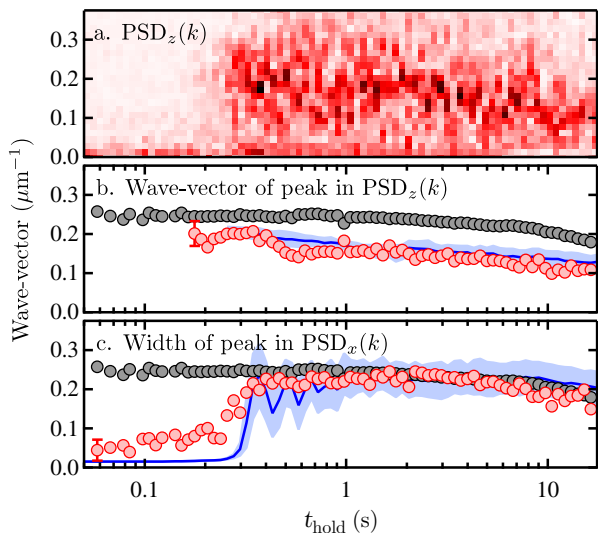


FIG. 4: Power spectral density. (a) $PSD_z(k)$ as a function of t_{hold} showing the formation of a peak at finite wave-vector k , followed by the gradual movement of that peak to smaller k as the spin domains expand. The color scale depicts increasing spectral power with darker color. (b) Wave-vector of $PSD_z(k)$'s peak. (c) Width of $PSD_x(k)$, which always peaked around zero. In both (b) and (c), the red symbols depict the experimentally observed peak location (typical uncertainty plotted on the leftmost point) and the blue curve plots the results of our SP-GPE simulation (uncertainties denoted by the blue band). In both cases, the uncertainties reflect the standard deviation over many realizations. The grey symbols mark $1/\xi_{1D}$, the homogenous-system wave-vector of maximum gain (the uncertainties are comparable to the symbol size). The oscillations for $t_{\text{hold}} < 1$ s in the simulation (blue curve, panel c) result from a damped breathing mode predominately along \mathbf{e}_z .

row peaks. By showing that the width of the peak in $PSD_x(k)$ tracks the inverse spin-healing length, Fig. 4c demonstrates that the domain walls are sized according to ξ_{1D} (grey symbols).

Because the $\approx 2\xi_{1D}(z)$ minimum domain size increases as the condensate depletes away, it is plausible that the increase in domain-size results from an increasing cut-off in the minimum domain size. We exclude this model by comparing ξ_{1D}^{-1} computed in the BEC's center (Fig. 4, grey symbols) to the wave-vector of the peak in $PSD_z(k)$; Fig. 4 plots experimental data with red symbols and SP-GPE simulation with the blue curve. They follow quite different time-dependences, with the domains growing rapidly at short times before ξ_{1D} appreciably changes, indicating that ξ_{1D} is not simply related to the typical domain size.

We conclude instead that we observe genuine coarsening of the domains resulting from dynamical exchange of particles between stable domains. On the basis of our data, we cannot identify the origin of this coarsening, but our SP-GPE simulations suggest that spin transport

through the uncondensed (thermal) fraction, not quantum tunneling, is the leading mechanism at our temperature.

For $c_2 < 0$, as in ^{87}Rb , Eqs. (1) and (2) allow us to describe our system's spin degree of freedom as a single component attractive BEC (while the overall density follows the conventional Thomas-Fermi profile). In our binary mixture, the process of domain formation is a spinor analog to the “chain of pearls” pattern that forms in 1D BEC's quenched from repulsive to attractive interactions [20, 21]. In that case, the growth of structure results from a modulational instability with peak gain at $k = 1/\xi$ set by the conventional healing length. Attractive Bose systems are intrinsically unstable against collapse [22], however, in our spinor system, any eventual collapse is stymied by an effective hard core interaction resulting from the strictly bounded individual spin wavefunctions, and higher order interaction terms omitted from Eq. (2).

Thus, in this binary spin system, we observe the full gamut of time scales starting with the rapid dynamical generation of spin-domains from an initially non-equilibrium system followed by their subsequent relaxation to progressively larger domains, i.e., coarsening. In this model, the coalescence of domains minimizes the attractive energy by maximizing the spatial extent of regions with the same spin. Indeed, the ground state consists of just two domains – one for each spin – thereby reducing to one the number of domain walls. The domains increase in size very slowly in time, but due to the overall decrease in the BEC's atom number, we cannot distinguish between different functional forms.

We appreciate discussions with and terminology introduced by N. Bray-Ali, and insight gleaned from C. Raman. We acknowledge the financial support the NSF through the Physics Frontier Center at JQI, and the ARO with funds from both the Atomtronics MURI and DARPA's OLE Program.

-
- [1] M. Greiner, O. Mandel, T. Esslinger, T. Hänsch, and I. Bloch, *Nature* **415**, 39 (2002).
 - [2] M. Greiner, O. Mandel, T. W. Hansch, and I. Bloch, *Nature* **419**, 51 (2002).
 - [3] J. Sebby-Strabley, B. L. Brown, M. Anderlini, P. J. Lee, W. D. Phillips, J. V. Porto, and P. R. Johnson, *Phys. Rev. Lett.* **98**, 200405 (2007).
 - [4] S. Will, T. Best, U. Schneider, L. Hackermuller, D.-S. Luhmann, and I. Bloch, *Nature* **465**, 197 (2010).
 - [5] D. M. Stamper-Kurn and M. Ueda, arXiv:1205.1888.
 - [6] A. Putnis, *An Introduction to Mineral Sciences* (Cambridge University Press, 1992).
 - [7] T. W. B. Kibble, *J. Phys. A: Math. Gen.* **9**, 1387 (1976).
 - [8] P. Calabrese, F. H. L. Essler, and M. Fagotti, *Journal of Statistical Mechanics: Theory and Experiment* **7**, P07016 (2012).
 - [9] R. Barnett, A. Turner, and E. Demler, *Phys. Rev. Lett.*

- 97**, 180412 (2006).
- [10] Y. Kawaguchi and M. Ueda, *Phys. Rev. A* **84**, 053616 (2011).
- [11] D. M. Weld, P. Medley, H. Miyake, D. Hucul, D. E. Pritchard, and W. Ketterle, *Phys. Rev. Lett.* **103**, 245301 (2009).
- [12] M. Hofer, J. Chang, C. Hamner, and P. Engels, *Phys. Rev. A* **84**, 041605 (2011).
- [13] D. S. Hall, M. R. Matthews, J. R. Ensher, C. E. Wieman, and E. A. Cornell, *Phys. Rev. Lett.* **81**, 1539 (1998).
- [14] K. M. Mertes, J. W. Merrill, R. Carretero-González, D. J. Frantzeskakis, P. G. Kevrekidis, and D. S. Hall, *Phys. Rev. Lett.* **99**, 190402 (2007).
- [15] J. Stenger, S. Inouye, D. M. Stamper-Kurn, H. J. Miesner, A. P. Chikkatur, and W. Ketterle, *Nature* **396**, 345 (1998).
- [16] W. Zhang, D. L. Zhou, M.-S. Chang, M. S. Chapman, and L. You, *Phys. Rev. Lett.* **95**, 180403 (2005).
- [17] L. E. Sadler, J. M. Higbie, S. R. Leslie, M. Vengalattore, and D. M. Stamper-Kurn, *Nature* **443**, 312 (2006).
- [18] M. Vengalattore, J. Guzman, S. R. Leslie, F. Serwane, and D. M. Stamper-Kurn, *Phys. Rev. A* **81**, 053612 (2010).
- [19] E. Bookjans, A. Vinit, and C. Raman, *Phys. Rev. Lett.* **107**, 195306 (2011).
- [20] K. E. Strecker, G. B. Partridge, A. G. Truscott, and R. G. Hulet, *Nature* **417**, 150 (2002).
- [21] S. E. Pollack, D. Dries, M. Junker, Y. P. Chen, T. A. Corcovilos, and R. G. Hulet, *Phys. Rev. Lett.* **102**, 090402 (2009).
- [22] E. A. Donley, N. R. Claussen, S. L. Cornish, J. L. Roberts, E. A. Cornell, and C. E. Wieman, *Nature* **412**, 295 (2001).
- [23] T.-L. Ho, *Phys. Rev. Lett.* **81**, 742 (1998).
- [24] A. Widera, F. Gerbier, S. Fölling, T. Gericke, O. Mandel, and I. Bloch, *New Journal of Physics* **8**, 152 (2006).
- [25] Y.-J. Lin, A. R. Perry, R. L. Compton, I. B. Spielman, and J. V. Porto, *Phys. Rev. A* **79**, 063631 (2009).
- [26] W. Gerlach and O. Stern, *Zeitschrift für Physik A* **9**, 349 (1922).
- [27] P. B. Blakie, A. S. Bradley, M. J. Davis, R. J. Ballagh, and C. W. Gardiner, *Advances in Physics* **57**, 363 (2008).
- [28] Except where otherwise stated, all uncertainties herein reflect the uncorrelated combination of single-sigma statistical and systematic uncertainties.
- [29] Our dipole trap is formed from a pair of axially symmetric 1064 nm laser beams intersecting at right angles with $1/e^2$ radii $\approx 67 \mu\text{m}$ and $\approx 300 \mu\text{m}$.
- [30] The $180 \mu\text{m}$ axial radius is not small compared to dipole laser's $300 \mu\text{m}$ waist along the axial direction; as a result, we expect small deviations from the conventional inverted parabola density profile.
- [31] We can apply a brief rf pulse just before TOF to partially re-populate $|m_F=0\rangle$; following TOF expansion and Stern-Gerlach separation, the distribution of all three spin states contains sufficient information to obtain M_x and M_z simultaneously.
- [32] The axial magnetic field in our system has a very small residual gradient $\nabla_z B = \gamma z$, where $\gamma = 0.092(4) \text{ G/cm}^2$, leads to small, but repeatable large-scale structure in $M_z(z)$. Although small, we can further mitigate the effects of this contribution with a spin echo π -pulse, flipping between $|\downarrow\rangle \leftrightarrow |\uparrow\rangle$ midway between the quench and the beginning of TOF. This inverts the effect of any inhomogeneous magnetic fields, but leaves the spin dynamics otherwise unaffected.